J Neurophysiol 105: 2601–2609, 2011.
First published February 23, 2011; doi:10.1152/jn.00722.2010.

Bulk electroporation and population calcium imaging in the adult mammalian retina

Kevin L. Briggman[1] and Thomas Euler[1,2]

[1]*Department of Biomedical Optics, Max Planck Institute for Medical Research, Heidelberg; and* [2]*Centre for Integrative Neuroscience (CIN) and Institute for Ophthalmic Research, University of Tübingen, Tübingen, Germany*

Submitted 18 August 2010; accepted in final form 22 February 2011

Briggman KL, Euler T. Bulk electroporation and population calcium imaging in the adult mammalian retina. *J Neurophysiol* 105: 2601–2609, 2011. First published February 23, 2011; doi:10.1152/jn.00722.2010.—The optical recording of light-evoked activity in populations of neurons in the mammalian retina offers several benefits over the use of multielectrode arrays. However, population imaging has been hindered by the effective loading of synthetic fluorescent indicators, especially in the mature tissue. We have therefore developed an electroporation method to label the complete ganglion cell layer of the adult mammalian retina. We optimized the protocol such that the retina recovers from electroporation and generates responses to visual stimuli. The method can be used with a diverse set of indicators with a range of affinities and emission wavelengths. It therefore can be combined with transgenic animals expressing fluorescent markers to target specific neuronal types. Importantly, the ganglion cell layer remains accessible for subsequent intracellular recording and morphological identification.

THE RECORDING OF POPULATIONS of neurons in the adult mammalian retina has been realized by the use of planar multielectrode arrays (MEAs) (DeVries and Baylor 1997; Litke et al. 2003; Meister et al. 1994). MEAs record precise spike-time information simultaneously from dozens of retinal ganglion cells (RGCs) and allow the recording of nearly complete mosaics from some subclasses of RGCs (DeVries and Baylor 1997; Field et al. 2009; Shlens et al. 2006). With state-of-the-art MEAs (512 electrodes) and advanced analysis techniques, even detailed functional measurements of RGC receptive field structure–down to the position of single cones–are possible (Field et al. 2007, 2010). A limitation of commercially available MEAs is the inability to unequivocally identify/locate the somata generating the recorded spikes. Although this problem may in the future be ameliorated by the arrival of high-resolution MEAs (Eversmann et al. 2003; Hutzler et al. 2006; Lambacher et al. 2004), other limitations are more serious. Because recordings are made with the ganglion cell layer (GCL) attached to the electrode, direct access for subsequent intracellular recording or iontophoretic dye filling is lost. Furthermore, the isolation of spikes attributable to individual neurons is probably biased toward neurons that generate large action potentials (APs) (Segev et al. 2004), have larger somata, and/or are located closer to the MEA surface. For instance, when reconstructed from MEA recordings, the mosaics of the smaller midget RGCs tend to be incomplete compared with those from larger RGCs (e.g., Gauthier et al. 2009).

Address for reprint requests and other correspondence: K. L. Briggman, Dept. of Biomedical Optics, Max Planck Institute for Medical Research, Jahnstrasse 29, 69120 Heidelberg, Germany (e-mail: briggman@mpimf-heidelberg.mpg.de).

These limitations of MEA recording can be overcome by using optical population imaging, albeit usually at the expense of spike-timing precision. Several protocols have been developed to label the GCL of the vertebrate retina with synthetic fluorescent calcium indicators, including optic nerve backfilling (Behrend et al. 2009; Zhan and Troy 1997), ballistic "gene-gun" delivery (Kettunen et al. 2002; Morgan and Wong 2008), and multicell bolus loading with membrane-permeable indicators (Blankenship et al. 2009). Although some of these protocols were aimed toward the sparse labeling of GCL neurons, those that sought uniform labeling work in the immature retina but have been unsuccessful at labeling the adult mammalian retina. Molecular methods with genetically encoded fluorescent biosensors (Miyawaki et al. 1997; Persechini et al. 1997) label multiple ganglion cells (Hasan et al. 2004) or interneurons (Dorostkar et al. 2010) in the adult retina but require the use of specific transgenic animals.

Our goal was to develop a technique to uniformly label all neurons within the GCL, both RGCs and displaced amacrine cells (dACs), using a reproducible and minimally invasive approach that maintains the light responsiveness of the adult mammalian retina. To achieve this, we developed a bulk electroporation protocol that uniformly labels the adult mouse GCL. We demonstrate that the retina recovers from the electroporation and generates the expected responses to visual stimuli. Moreover, the protocol is both rapid and simple to implement.

MATERIALS AND METHODS

Solutions and dyes. As standard medium, we used for tissue dissection, electroporation, and recordings a commercially available saline (Biometra, Göttingen, Germany) that was supplemented with 0.5 mM L-glutamine and carboxygenated (95% O_2-5% CO_2). As noted previously, the addition of glutamine was essential for normal on and off responses (Ames and Nesbett 1981). To visualize the retinal morphology under the two-photon (2P) microscope and to stain for damaged cells (Euler et al. 2009; Schlichtenbrede et al. 2009), we added sulforhodamine 101 (SR101; final concentration 0.5–1 μM; Sigma-Aldrich, Munich, Germany) to the superfusion medium. For the electroporation, a 5 mM solution (in saline) of the synthetic calcium indicator dye Oregon Green 488 BAPTA-1 (OGB-1; hexapotassium salt; Invitrogen, Darmstadt, Germany) was used for most experiments. In some experiments, we also electroporated 5 mM Oregon Green 488 BAPTA-2 octapotassium salt, Oregon Green 488 BAPTA-6F hexapotassium salt, or rhod-2 tripotassium salt (all from Invitrogen).

Animals and tissue preparation. Wild-type (C57BL/6) mice (≥4 wk old) were dark-adapted for at least 2 h before the experiment. All subsequent procedures were carried out under dim red illumination. The animals were anesthetized with isoflurane (Baxter, Unter-

0022-3077/11 Copyright © 2011 the American Physiological Society

schleißheim, Germany) inhalation and killed by cervical dislocation. The eyes were enucleated and transferred to a dish containing carboxygenated room-temperature saline, in which the retinas were dissected. All procedures were approved by the local animal care committee and were in accordance with the law of animal experimentation issued by the German Federal Government.

Electroporation parameters. The optimized electroporation parameters for whole-mounted retina on filter paper (0.8-μm black; AABP; Millipore, Schwalbach, Germany) were +13-V (top electrode, on GCL side), 10-ms-pulse-width, 1-Hz-pulse-frequency, 10-square-wave pulses monitored with an oscilloscope (see also RESULTS). Comparable results were achieved both with a specialized electroporator (CUY21; Nepagene/BioVendor, Heidelberg, Germany) and a combination of pulse generator (TGP110) and wide-band amplifier (WA301; both from Thurlby Thandar/Farnell, Oberhaching, Germany; 50-Ω output).

2P microscopy. For 2P imaging (Denk et al. 1990), we used a custom-built microscope ["eyecup scope" (Euler et al. 2009)]. In brief, the eyecup scope was equipped with through-the-objective light stimulation and two detection channels for fluorescence imaging (red, HQ 622 BP 36, and green, D 535 BP 50 or 520 BP 30; AHF/Chroma, Tübingen, Germany). The excitation source was a mode-locked Ti/sapphire laser (Mira-900; Coherent, Dieburg, Germany) tuned to ~930 nm. The microscope was used to simultaneously visualize the retinal structure with SR101 (red channel; see above) and to monitor calcium activity reflected by OGB-1 fluorescence changes (green channel). Typical scan parameters were [pixels/line $\times$ lines (frame rate in Hz)]: 64 $\times$ 64 (7.8), 128 $\times$ 128 (3.9), and 256 $\times$ 256 (2.0), each at 2 ms/line. A marker signal coming from the light stimulator (see *Electrical recordings*) was acquired (at 500 Hz) with the image data to allow synchronizing calcium signals with stimulus presentations.

Electrical recordings. Spike trains were extracellularly recorded from RGCs in loose-patch configuration using patch pipettes (5–15 MΩ, borosilicate, outer diameter: 1.0 mm, inner diameter: 0.58 mm, with filament; Hilgenberg) filled with saline containing 15 mM SR101. In the case of electrical recordings, we omitted the SR101 from the bathing saline and targeted an OGB-1-labeled cell with the electrode under visual control (2P imaging), using fluorescence from the SR101 leaking out of the electrode to visualize the approach. Data were acquired using a Multiclamp amplifier (with Digidata 1322A and pClamp8 software; Molecular Devices, Berkshire, United Kingdom), digitized (5 kHz), low-pass filtered (2 kHz), and analyzed offline using custom MATLAB (MathWorks, Natick, MA) software. After the recording, we broke into the cell (typically using 2–8 1-ms pulses of 10 mV). The cells filled with SR101 by diffusion from the electrode within minutes, and their morphology was then recorded by taking image stacks.

Light stimulation. Our light stimulator used custom-written software running on a personal computer (with Windows XP; Microsoft) to present spatially and temporally structured stimuli on an 800- $\times$ 600-pixel miniature liquid crystal on silicon (LCoS) display (i-glasses; EST, Kaiserslautern, Germany), alternately illuminated by two band-pass-filtered (blue: 400 BP 20, green: 578 BP 10; AHF/Chroma) light-emitting diodes (LEDs) within each frame (for details, see Euler et al. 2009). The intensity ranges for the blue and green stimulus components were (as irradiance in 10^3 photons$\cdot s^{-1}\cdot\mu m^{-2}$) 35–283 and 10–283, respectively. Although color stimuli were supported, we restricted the stimuli used here to "gray" stimuli (with both blue and green at the same intensity). The LCoS display was coupled into the main optical path of the microscope, and hence the stimuli were projected onto the retina through the objective lens (XLUMPlanFl 20 $\times$ 0.95 numerical aperture, water-immersion; Olympus). We used two kinds of stimuli: a series of flashed spots of increasing diameter (50–800 μm) and a bar (300 $\times$ 1,000 μm) moving in eight different directions at 0.5 mm/s. In both cases, the stimulus had a positive contrast (bright on darker background).

Data analysis. Images were analyzed offline using custom MATLAB software. In brief, circular regions of interest (ROIs) cells were manually placed on all cells in a field-of-view, and the pixel intensities within a ROI were averaged at each time step. The fractional fluorescence changes were calculated using the mean intensity of each ROI across an entire recording trial as the baseline. The responses to individual stimulus presentations were extracted using the marker signal from the stimulator embedded in the image stacks.

RESULTS

We aimed to develop a parallel plate electroporation method to reliably and uniformly label the GCL of the mouse retina with synthetic fluorescent calcium indicators. Our strategy was first to achieve uniform labeling across the GCL and then to adjust the electroporation parameters to ensure normal light-evoked responses from RGCs. We routinely employ 2P microscopy (Denk et al. 1990) to record light-stimulus-driven activity in the retina (Denk and Detwiler 1999). We used a custom upright microscope, the eyecup-scope (Euler et al. 2009), to image whole-mount retinas mounted photoreceptor side down onto filter paper. Arranging the retina in this orientation allows simultaneous 2P imaging during the projection of a stimulus, through the objective lens, onto the photoreceptors. This way, the GCL is also accessible for intracellular physiology (e.g., Euler et al. 2002).

Because we wanted to preserve this recording configuration, we chose a commercial electroporation dish/electrode pair (CUY700P3E/L; Nepagene/Xceltis, Meckesheim, Germany) consisting of horizontal, flat, 3-mm-diameter electrodes (Fig. 1*A*). An explanted mouse retina was hemisected, and one half was mounted photoreceptor side down on filter paper (see MATERIALS AND METHODS). The well of the electroporation dish containing the lower electrode was filled with 7 μl of saline. The retina was then centered over the lower electrode, and excess saline was wicked away from the filter paper with a Kimwipe. A 5-μl drop of the fluorescent indicator dissolved in saline was applied to the underside of the upper electrode. The upper electrode, mounted on a micromanipulator, was lowered until the drop was in contact with the retina. The distance between the two electrodes was 2 mm. Note that the repeatable positioning of the upper electrode is critical for reproducible results. The retina was then electroporated, the upper electrode raised, and the filter paper with the attached retina transferred to the warmed (30–32°C) recording chamber in the eyecup-scope, where the tissue was superfused (at ~3 ml/min) with carboxygenated saline. The total time between contacting the retina with the indicator solution until it was placed in the recording chamber was <20 s.

We optimized 4 electroporation parameters for uniform labeling of the GCL: pulse width, pulse frequency, number of pulses, and applied voltage. Preliminary experiments suggested that a 5 mM concentration of Oregon Green BAPTA-1 hexapotassium salt is sufficient to achieve intense labeling of GCL somata. Our initial goal was to obtain uniform labeling of all cell bodies within the GCL across the area exposed to the electric field. This was easily achieved using many brief, high-frequency square-wave pulses (initially we used +20 V, 1-ms pulses, 100 Hz, 100 pulses). Although we observed strong labeling of the GCL with such a protocol, the retinas were not light responsive, and many of the neurons rapidly became unhealthy. Degradation of neuron health was assessed

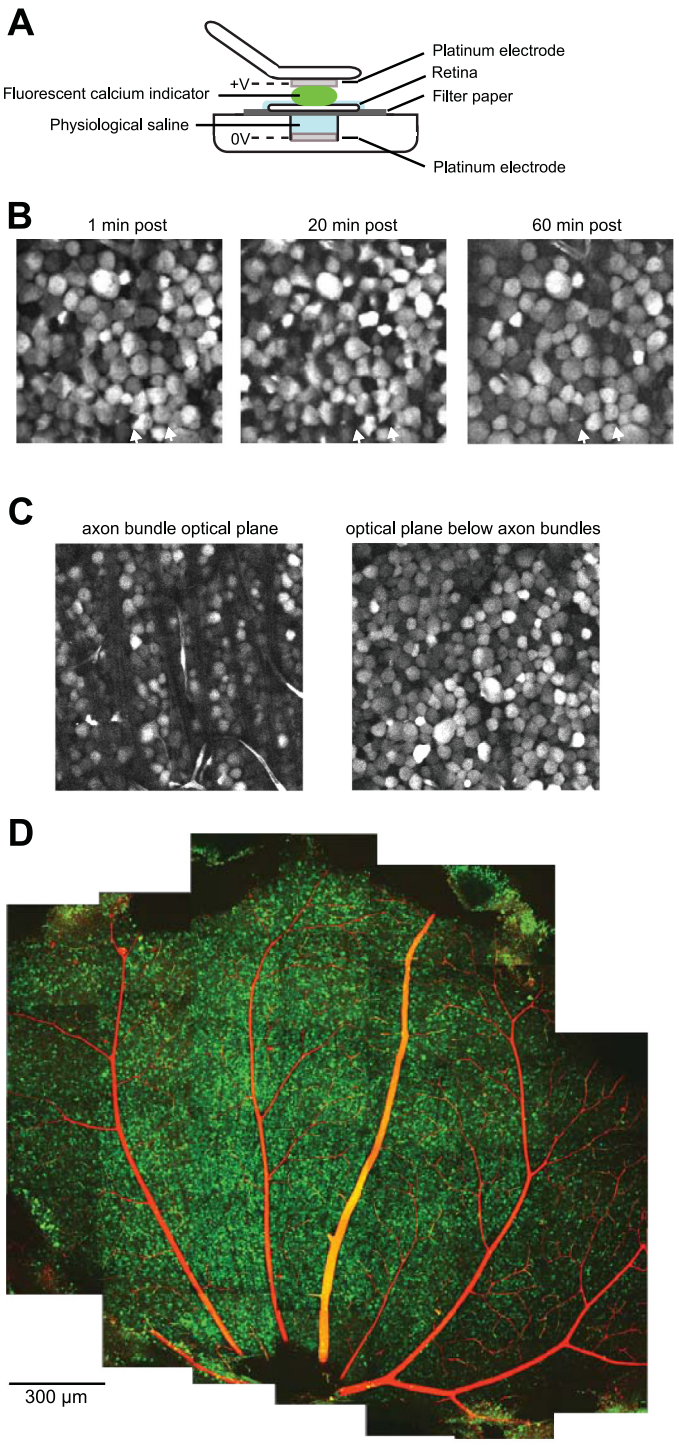

Fig. 1. Electroporation and the resulting tissue labeling. *A*: schematic drawing showing vertical cross-section of electroporation configuration. *B*: 2-photon (2P) micrographs of a whole-mounted mouse retina 1 (*left*), 20 (*middle*), and 60 min (*right*) after electroporation with Oregon Green 488 BAPTA-1 [OGB-1; focal plane in ganglion cell layer (GCL), only green channel shown]. White arrows indicate examples of Müller cell endfeet, which are swollen in the *middle* but not anymore on the *right*. *C*: different focal planes illustrating that axon bundles do not hinder labeling or imaging. *D*: montage of 2P micrographs [green, OGB-1; red, sulforhodamine 101 (SR101)] of whole-mounted mouse retina with optic disc at the lower edge center of picture.

by observing neurons fill with an extracellular polar tracer dye in the bath, SR101 (see also Euler et al. 2009; Schlichtenbrede et al. 2009). We subsequently modified the protocol to use fewer brief, low-frequency pulses, a strategy that has been used to optimize loading of mammalian cells with small molecules (Rols and Teissie 1998). This change still allowed us to label the GCL uniformly and also record light-evoked responses (see below). The optimized protocol parameters were +13 V, 10-ms pulse width, 1-Hz pulse frequency, 10 square-wave pulses. Using this protocol, we did not observe neurons in the GCL (or in the other retinal layers) fill with SR101 following the electroporation (Fig. 1*D*). Moreover, subsequent electron microscopy of electroporated and calcium-imaged retina does not reveal any ultrastructural damage or prevent the reconstruction of complete neurons (see Briggman et al. 2011). Although we did not perform an exhaustive search of the parameter space, we found the labeling quality to be robust to at least 10% deviations in any of the parameters. Because we focused primarily on varying voltage and pulse length while testing only few values for electrode distance, pulse number, and pulse frequency, our protocol is optimized only within a local region of the large parameter space. We initially used a commercial electroporation apparatus (CUY21 electroporator; see MATERIALS AND METHODS) for optimizing parameters. The low voltage of the final protocol allowed us, however, to use a simple (and less expensive) combination of a general purpose pulse generator with a wide-band amplifier.

Immediately following electroporation, we placed the retina in the eyecup-scope and acquired images of the GCL. A successful electroporation showed an initial intense labeling of GCL somata and no labeling of the inner nuclear layer (INL) or photoreceptor layers (Fig. 1*B*, *left*). A recovery period of 45–60 min in the heated, superfused chamber followed. During this period, the Müller cell endfeet swell as the retina presumably recovers from electroporation (Fig. 1*B*, *middle*, white arrows indicate swollen endfeet). Following the recovery period, swelling subsided, and OGB-1-filled somata within the GCL appeared healthy (based on their shape and the exclusion of SR101; Fig. 1*B*, *right*). Müller cell somata in the INL were OGB-1-labeled following the recovery period presumably due to diffusion from the electroporated endfeet in the GCL. This protocol leads to uniform labeling horizontally across the GCL (Fig. 1, *C* and *D*). We observed some variability in the fluorescence intensity among GCL cells, likely caused by differences in the intracellular dye concentration and/or resting calcium levels. Bundles of axons running over the surface of the GCL did not present a barrier to electroporation because we routinely observed underlying somata filled with the indicator (compare Fig. 1*C*, *left* vs. *right*). Also, we found no obvious correlation between soma size or responsiveness to light and fluorescence intensity.

We stimulated the retinas by projecting patterned light stimuli through the objective onto the plane of the photoreceptor outer segments (for details on light stimuli, see MATERIALS AND METHODS and Fig. 2). In light-responsive retinas, an on response was detected from many of the cells within a field of view at the onset of scanning with the 2P laser beam (data not shown) presumably due to photoreceptor excitation by the infrared laser light and by indicator fluorescence (compare Euler et al. 2009). Following a 5- to 10-s delay that allowed the retina to adapt to the laser-induced response, a light stimulus

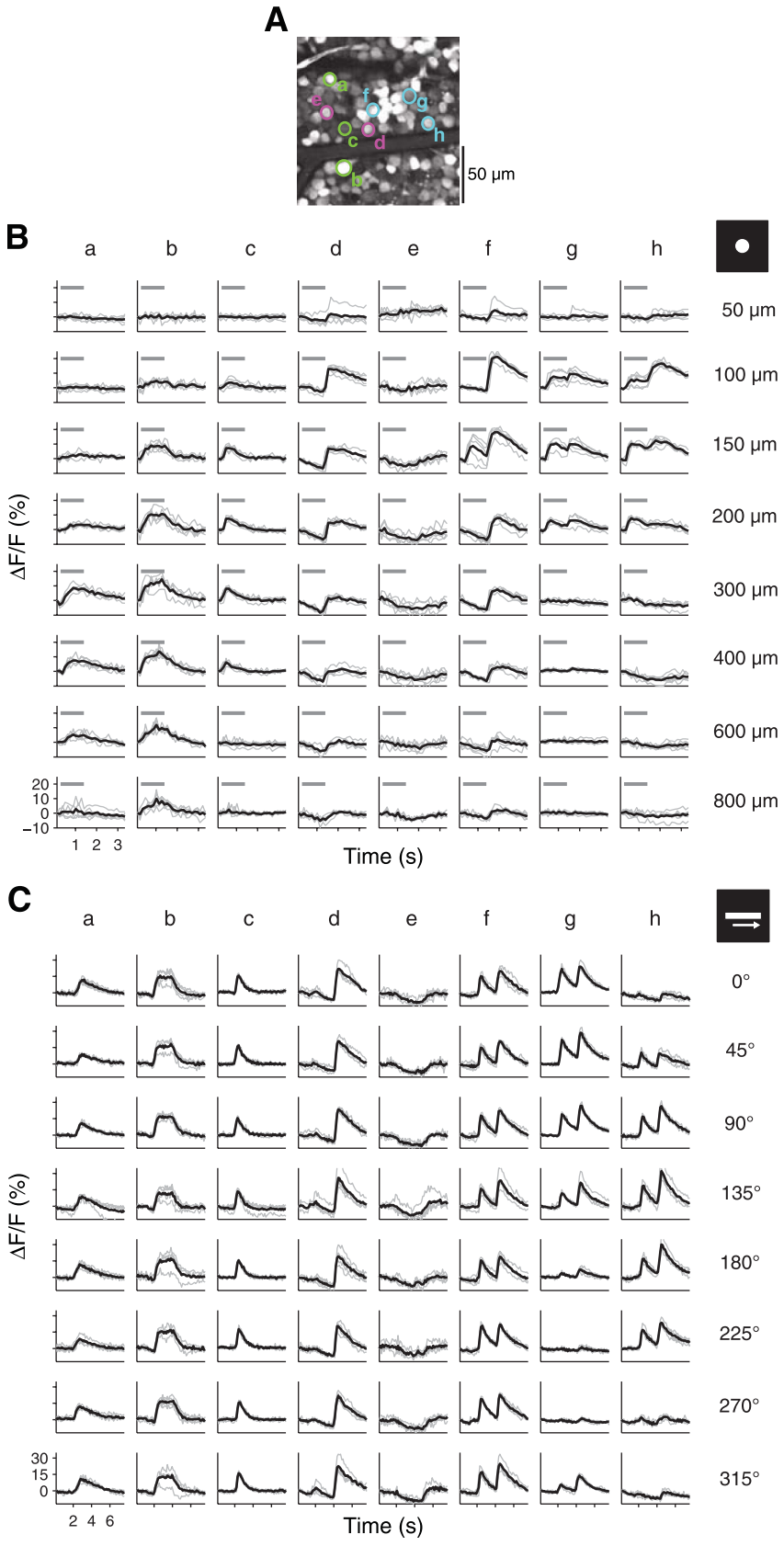

Fig. 2. Examples for calcium signals from selected cells in the GCL. *A*: overview showing imaged retinal region (focus in GCL, only green channel) with regions of interest (ROIs) on 8 representative somata. *B*: fractional changes in calcium signals (ΔF/F) evoked by flashed bright spots with increasing diameters (as indicated to the *right* of the traces) in the cells highlighted in *A*. Average (black traces) and single trials (n = 5, gray traces) are shown. *C*: calcium responses in same set of cells (as in *A* and *B*) but to a bright bar moving in 8 different stimulus directions (as indicated to the *right* of the traces).

was projected onto the retina. To account for possible differences in adaptation/light sensitivity between preparations, we determined an optimal contrast level (typically 40–60% contrast) for each retina piece by projecting a white spot on a gray background and measured calcium transient magnitudes from several test cells (including on, off, and on/off cells) within an initial field of view as we incremented the contrast between the spot and background. The optimal foreground/background contrast at which we observed the largest stimulus-induced signals from a majority of the test cells was used for the remainder of the experiment.

We observed a variety of response types, including on, off, and on/off responses to a light spot, as demonstrated by a selection of eight representative neurons visible within one field of view (Fig. 2*A*). We measured receptive field sizes for each neuron (Fig. 2*B*) in response to a spot of increasing diameter. The continuous scanning of the 2P laser beam therefore did not appear to have disrupted our ability to resolve the expected response properties of GCL neurons (Euler et al. 2009). Furthermore, there was little variability between repeated presentations of the same stimuli (Fig. 2, *B* and *C*). Responses of the same neurons to a moving bar stimulus confirmed this repeatability and demonstrated the ability to distinguish directionally selective RGCs (Fig. 2*C*; *cells g* and *h*) (reviewed in Euler and Hausselt 2008).

The same electroporation protocol was used to successfully load indicators of different affinities (Fig. 3, *A* and *B*) and emission wavelengths (λ_{em}) (Fig. 3*C*) including: OGB-2 (K_d = 580 nM, λ_{em} = 520 nm), OGB-6F (K_d = 3 μM, λ_{em} = 520 nm), and rhod-2 (K_d = 580 nM, λ_{em} = 580 nm). Cells loaded with these indicators were responsive to the moving bar stimulus (Fig. 3, *bottom*). However, we consistently observed the largest fractional changes (Fig. 2) with OGB-1 (K_d = 170 nM, λ_{em} = 520 nm) and so used it for the following experiments.

To further test the integrity of the retinal circuitry following electroporation, we performed extracellular loose-patch recordings of RGCs (Fig. 4). The recorded cells typically displayed light-evoked spiking responses, as illustrated by an off RGC recorded simultaneously with calcium imaging (Fig. 4, *A–C*) and an on/off direction-selective RGC recorded following calcium imaging (Fig. 4, *D–F*). Generally, spiking responses correlated to the presence of calcium transients. Furthermore, the directional tuning curves for the direction-selective RGC were similar when plotted using the number of spikes or the integrated calcium transients (Fig. 4*E*). Following extracellular recording, we juxtacellularly filled both cells with SR101, and the resulting morphologies were consistent with the observed physiology, an off RGC (Fig. 4*C*) and an on/off RGC (Fig. 4*F*). The firing rates we observed for the on/off direction-selective RGC are consistent with the photopic stimulation of mouse on/off direction-selective RGCs in nonelectroporated retina (e.g., Weng et al. 2005).

We also quantified the fraction of neurons exhibiting each response type (on, off, and on/off) as well as the percentage of nonresponsive (NR) neurons (those without changes in baseline fluorescence intensity; Fig. 5*A*). We expected to find some NR neurons due to the presence of dACs in the GCL as well as the assumption that most of them will not generate bursts of somatic APs and therefore possibly lack detectable somatic calcium signals (Oesch et al. 2005). The percentage of NR neurons, 35%, is less than the estimated fraction of dACs in the mouse retina, 59% (Jeon et al. 1998), suggesting that we recorded responses from a fraction of dACs (Fig. 5*B*). Although we cannot rule out that some of the NR neurons were not adequately filled and/or rendered unresponsive due to the electroporation, the overall fraction of light-responsive cells (65%) suggests that this was not the case for a significant fraction of neurons.

We routinely scanned areas of 100 by 100 μm, which was a reasonable tradeoff between frame rate (7.8 Hz) and the number of cells simultaneously recorded in a field of view (usually 50–70 neurons). To acquire responses from hundreds of neurons, we tiled a region of the retina, delivering stimuli centered on each tile. A 3 × 3 tiling covers a region of 300 by 300 μm and samples approximately 450–650 neurons (Fig. 5*C*). Such tiling allowed us to identify functional mosaics, such as those created by directionally selective RGCs (Fig. 5*D*). This demonstrates that even though the intracellular dye concentration likely varied between GCL cells, our method can yield "functionally" uniform labeling.

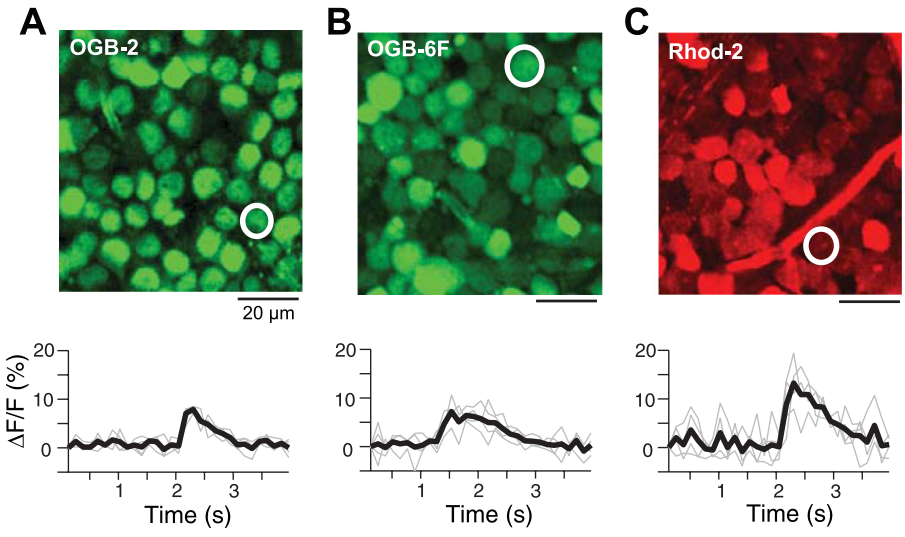

Fig. 3. Electroporation of different calcium indicators. 2P micrographs of whole-mounted mouse retina electroporated with OGB-2 (*A*), OGB-6F (*B*), and rhod-2 (*C*). The false coloring reflects the difference in the emission wavelength of the indicator dyes. *Bottom* are example traces of light-evoked calcium transients (ΔF/F) from the highlighted cells (white circles). The stimulus was a moving bar sweeping across the field of view (as in Fig. 2*C*). Average (black traces) and single trials (n = 5, gray traces) are shown. Scale bar = 20 μm.

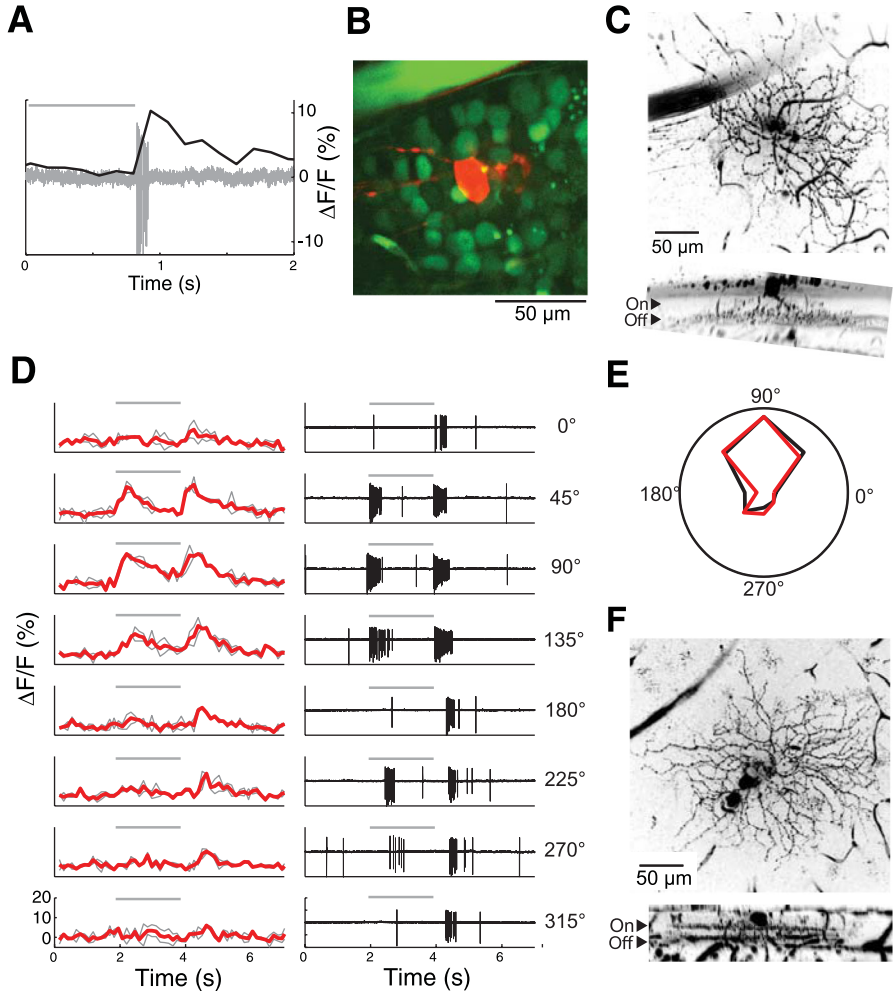

Fig. 4. Electrical responses from calcium indicator-loaded retinal ganglion cells (RGCs). *A*: simultaneous imaging and extracellular recording of an off RGC in responses to a moving bar stimulus. *B*: juxtacellular filling of the soma of the cell in *A* with SR101 (red). *C*: maximum intensity projection (*top*) and vertical reslice (*bottom*) of an image stack of the cell from *A* and *B*. Note the dendritic stratification in the distal half of the inner plexiform layer is consistent with an off RGC. *D*: calcium signals from an on/off direction-selective RGC (*left*) in response to a moving bar stimulus (see Fig. 2*C*). On a subsequent nonimaging trial, the extracellular spiking responses to the same stimulus were recorded (*right*). *E*: the directional tuning curves for the cell in *D*, as polar plots using either the total spike counts for the on and off responses (black curve) or the total integrated area under the calcium transients (red curve). Both curves were normalized to the respective peak response. *F*: maximum intensity projection (*top*) and vertical reslice (*bottom*) of the cell from *D* and *E*. Note the morphology is consistent with a bistratified on/off direction-selective RGC.

DISCUSSION

Comparison with other population recording techniques. MEA recording is currently the standard method to acquire population responses from explanted, whole-mount retinas (Litke et al. 2003). MEAs provide the ability to record precise spike-timing information across large RGC populations and have been used to resolve receptive field mosaics (Field et al. 2009, 2010; Shlens et al. 2006, 2009). Optical population recordings offer several advantages over MEA recordings. Perhaps most importantly, GCL neurons are directly accessible for subsequent single cell characterization such as intracellular dye filling or patch-clamp recording (Fig. 4). Unlike MEAs, in which the position of a soma that is generating spikes is inferred from electrode positions and receptive field location (Field et al. 2009), the soma location in optical imaging is intrinsically defined. Therefore, optical imaging also allows the study of retinal regions where the cells in the GCL are most densely packed and may occupy multiple layers (like in the area centralis or in the fovea). Here, current MEA techniques fail. The thin optical sectioning ability of 2P imaging allows us to exclude passing axons from the focal plane. Therefore, potential signals from these axons do not contaminate the responses from identified somata, allowing recording from regions of high axon density, including regions near the optic disk or near specialized areas, such as the area/fovea centralis. In any case, we rarely observed substantial labeling of axon bundles following electroporation (Fig. 1*C*). Finally, although MEA recording is biased toward RGCs generating large spikes, calcium imaging in principle also allows the detection of subthreshold voltage fluctuations that cause an influx of calcium (Canepari et al. 2008). The fraction of neurons that generated calcium transients in our recordings (Fig. 5, *A* and *B*) suggest we were recording some dACs, most of which would probably remain undetectable with MEA recording (Segev et al. 2004).

A major limitation of high-affinity indicators, such as OGB-1 (K_d = 170 nM), is the slow fluorescence decay time constant of calcium signals in response to APs (approximately hundreds of milliseconds; reviewed in Hendel et al. 2008). Because RGCs generate bursts of spikes, recovering precise times for individual spikes is hindered by the decay time constant. Although it is possible to reconstruct firing rates of bursting neurons with a deconvolution-based technique (Yaksi and Friedrich 2006), this technique has a limited interburst resolution of ~30 ms (due to multiple factors, including the indicator decay time constant). The ability to accurately deconvolve rapid firing-rate changes also requires a higher frame rate [125 Hz (Yaksi and Friedrich 2006)] than the maximal rate we have used here (7.8 Hz). We instead chose to sacrifice frame rate to increase the number of neurons per field of view while maintaining high signal-to-noise ratios. This enabled us to physiologically characterize large numbers of cells with only

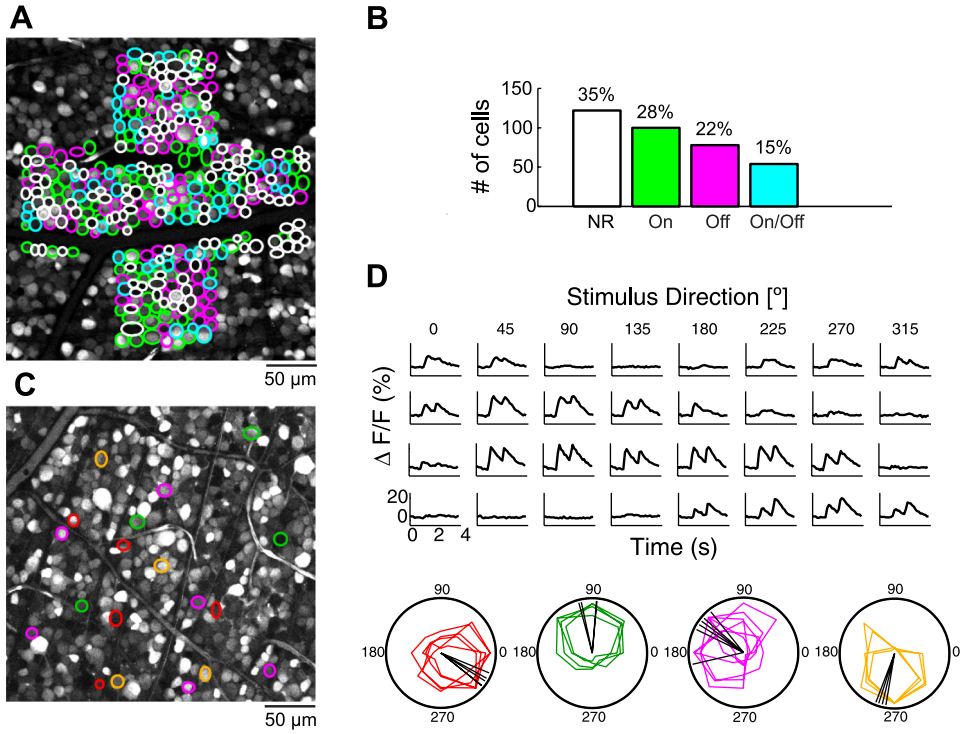

Fig. 5. Responsive vs. nonresponsive (NR) cells and a functional mosaic of a RGC population. *A*: overview image of 5 fields of view (focus in GCL, only green channel) in which all somata are encircled. ROI color codes response type (on, green; off, magenta; on/off, blue) or the lack thereof (NR, white). *B*: histogram of cell frequency as a function of response type (as defined in *A*). *C*: overview image of 9 fields of view (focus in GCL, only green channel) with all direction-selective (DS) RGCs encircled; ROI color codes the preferred direction of the cells (see *D*, *bottom*). *D*, *top*: average calcium responses (ΔF/F) to the directions of the moving bar stimulus for 4 cells. *Bottom*: polar plots showing the total integrated area under the average response for each cell as a function of stimulus direction. Each tuning curve is normalized to the peak directional response for each cell. The polar plots corresponding to the cells circled in *A* were manually clustered by preferred direction (magenta, green, red, or orange). Black lines indicate the vector-summed response corresponding to the preferred direction.

a few stimulus presentations. With the exception of the correlations presented in Fig. 4, we have therefore not attempted to relate quantitatively the calcium transients we detect to simultaneously recorded spike trains. We, however, were able to clearly distinguish gross firing-rate characteristics such as whether the response is transient or sustained (Fig. 2*C*, *cell b* vs. *c*). Since with our method cell labeling intensity is high enough, increasing the frame rate is possible by decreasing the laser dwell time and/or the number of pixels per cell.

Comparison with other fluorescent indicator loading techniques. Several alternative approaches to bulk load retinas with fluorescent indicators have been reported, however, the loading of adult mammalian retina has proven difficult. Backfilling the optic nerve can selectively fill RGC axons and somata in the adult salamander retina (Behrend et al. 2009), but this approach was unsuccessful in the adult mammalian retina. A longer-duration backfilling protocol can label even peripheral RGCs in the adult mammalian retina (Zhan and Troy 1997) but requires long-term incubation (dozens of hours) not suitable for acute physiological recordings. At conditions that limit bullet-related tissue damage, ballistic delivery of indicator dyes to the isolated retina leads to only sparse labeling (approximately 1–15%) of neurons (Kettunen et al. 2002; Morgan and Wong 2008). Electroporation of the entire eyecup following indicator injection into the vitreous body also leads to only sparse labeling of neurons in the GCL (Yu et al. 2009). We observed such sparse labeling during our optimization of the protocol described here but did not pursue this direction because our goal was uniform labeling of the GCL.

A common method for bulk loading is the use of membrane-permeable AM forms of the indicator molecules. The multicell bolus loading technique labels the GCL of the retina (Blankenship et al. 2009) but requires substantial concentrations of DMSO and pluronic acid (Stosiek et al. 2003), both of which affect cell membrane integrity, presumably also beyond the staining period. AM loading also depends on the presence of the appropriate intracellular esterase to cleave the ester group, and labeling efficiency may therefore depend on cell type (Roe et al. 1990). Moreover, a side-effect of intracellular AM cleavage is the generation of formaldehyde (Tsien 1981). Sufficient loading in the retina requires penetration of the inner limiting membrane (ILM) with a micropipette and pressure ejection of the indicator resulting in local labeling of the GCL (Blankenship et al. 2009). Many such penetrations of the ILM would be necessary to label the same horizontal areas that we have described using bulk electroporation. Furthermore, although AM loading has been used for juvenile (postnatal *days 10–13*) mice (Blankenship et al. 2009), it has limited efficacy in adult retina (Wong and Oakley 1996). Because our final goal is to examine the ultrastructure of retinas from which we have recorded light stimulus-driven activity (Briggman et al. 2011), averting any tissue damage is pivotal. The use of parallel-plate electroporation electrodes obviates the need for detergents or to puncture the ILM with electrodes or bullets.

Comparison with other bulk-electroporation preparations. Local electroporation from a patch electrode has been used as an alternative for AM loading in different brain regions, leading to local (within a few tens of micrometers of the electrode) but complete filling of neurons (Nagayama et al. 2007). Our study was initially motivated by the use of bulk electroporation to label the neonatal mouse spinal cord in vitro (Bonnot et al. 2005). Similar to our experience, a recovery period following electroporation was necessary to regain normal circuit function (e.g., rhythmic locomotor activity reappeared 1–2 h after electroporation). Our optimized protocol for the retina uses a similar applied electric field (retina, 13 V/2 mm vs. spinal cord, 18–27 V/3 mm) to achieve dense labeling but shorter duration pulses (10 ms in

the retina vs. 50–100 ms in the spinal cord). Because of the similarity between these two protocols, it is possible that our protocol could be adapted to other flat-mountable tissues, such as acute brain slices.

Further applications. Although the functional recordings we described were performed using OGB-1, we have also successfully electroporated lower-affinity indicators (OGB-2, OGB-6F) and indicators with different emission wavelength (rhod-2, λ_{em} = 580 nm; Fig. 3). We chose OGB-1 because it shows large fractional fluorescence changes, but the use of lower-affinity indicators should allow the monitoring of faster firing-rate changes and reduce the risk of saturation (Yaksi and Friedrich 2006). The ability to electroporate, for example, red fluorescent indicators could be combined with genetically GFP-labeled RGCs to monitor activity across a population of genetically identified neurons (Siegert et al. 2009).

We optimized the protocol to achieve uniform labeling of the GCL across nearly the entire horizontal extent of the whole-mounted retina. Because of this uniformity, it is possible to monitor regional functional differences along dorsal-ventral or nasal-temporal axes of the retina, e.g., related to the opsin coexpression gradient in mice (Rohlich et al. 1994). Although we have focused on the differences to MEA recordings, the two techniques complement each other well and could even be combined, for example, to study lateral interactions in the retina that spread beyond the spatial extent of existing MEAs. Finally, because this protocol labels adult mouse retina, we expect it can also be adapted to other adult mammalian retinas, which have proven difficult to label otherwise. It remains to be seen whether the thicker ILM or nerve fiber layer of, for example, the primate retina affects labeling of the GCL as reported here.

ACKNOWLEDGMENTS

We thank Winfried Denk for useful comments on the manuscript.

GRANTS

This study was supported by the Max Planck Society and the Deutsche Forschungsgemeinschaft Grant EXC 307 (T. Euler).

DISCLOSURES

No conflicts of interest, financial or otherwise, are declared by the author(s).

REFERENCES

Ames A 3rd, Nesbett FB. In vitro retina as an experimental model of the central nervous system. *J Neurochem* 37: 867–877, 1981.

Behrend MR, Ahuja AK, Humayun MS, Weiland JD, Chow RH. Selective labeling of retinal ganglion cells with calcium indicators by retrograde loading in vitro. *J Neurosci Methods* 179: 166–172, 2009.

Blankenship AG, Ford KJ, Johnson J, Seal RP, Edwards RH, Copenhagen DR, Feller MB. Synaptic and extrasynaptic factors governing glutamatergic retinal waves. *Neuron* 62: 230–241, 2009.

Bonnot A, Mentis GZ, Skoch J, O'Donovan MJ. Electroporation loading of calcium-sensitive dyes into the CNS. *J Neurophysiol* 93: 1793–1808, 2005.

Briggman KL, Helmstaedter M, Denk W. Wiring specificity in the direction-selectivity circuit of the mouse retina. *Nature* 471: 183–188, 2011.

Canepari M, Vogt K, Zecevic D. Combining voltage and calcium imaging from neuronal dendrites. *Cell Mol Neurobiol* 28: 1079–1093, 2008.

Denk W, Detwiler PB. Optical recording of light-evoked calcium signals in the functionally intact retina. *Proc Natl Acad Sci USA* 96: 7035–7040, 1999.

Denk W, Strickler JH, Webb WW. Two-photon laser scanning fluorescence microscopy. *Science* 248: 73–76, 1990.

DeVries SH, Baylor DA. Mosaic arrangement of ganglion cell receptive fields in rabbit retina. *J Neurophysiol* 78: 2048–2060, 1997.

Dorostkar MM, Dreosti E, Odermatt B, Lagnado L. Computational processing of optical measurements of neuronal and synaptic activity in networks. *J Neurosci Methods* 188: 141–150, 2010.

Euler T, Detwiler PB, Denk W. Directionally selective calcium signals in dendrites of starburst amacrine cells. *Nature* 418: 845–852, 2002.

Euler T, Hausselt SE. Direction selective cells. In: *Vision I, The Senses: A Comprehensive Reference*, edited by Masland RH and Albright TD. San Diego, CA: Academic Press, 2008, p. 413–845–422.

Euler T, Hausselt SE, Margolis DJ, Breuninger T, Castell X, Detwiler PB, Denk W. Eyecup scope–optical recordings of light stimulus-evoked fluorescence signals in the retina. *Pflügers Arch* 457: 1393–1414, 2009.

Eversmann B, Jenkner M, Hofmann F, Paulus C, Brederlow R, Holzapfl B, Fromherz P, Merz M, Brenner M, Schreiter M, Gabl R, Plehnert K, Steinhauser M, Eckstein G, Schmitt-Landsiedel D, Thewes R. A 128x128 CMOS biosensor array for extracellular recording of neural activity. *IEEE J Solid-State Circuits* 38: 2306–2317, 2003.

Field GD, Gauthier JL, Sher A, Greschner M, Machado TA, Jepson LH, Shlens J, Gunning DE, Mathieson K, Dabrowski W, Paninski L, Litke AM, Chichilnisky EJ. Functional connectivity in the retina at the resolution of photoreceptors. *Nature* 467: 673–677, 2010.

Field GD, Greschner M, Gauthier JL, Rangel C, Shlens J, Sher A, Marshak DW, Litke AM, Chichilnisky EJ. High-sensitivity rod photoreceptor input to the blue-yellow color opponent pathway in macaque retina. *Nat Neurosci* 12: 1159–1164, 2009.

Field GD, Sher A, Gauthier JL, Greschner M, Shlens J, Litke AM, Chichilnisky EJ. Spatial properties and functional organization of small bistratified ganglion cells in primate retina. *J Neurosci* 27: 13261–13272, 2007.

Gauthier JL, Field GD, Sher A, Shlens J, Greschner M, Litke AM, Chichilnisky EJ. Uniform signal redundancy of parasol and midget ganglion cells in primate retina. *J Neurosci* 29: 4675–4680, 2009.

Hasan MT, Friedrich RW, Euler T, Larkum ME, Giese G, Both M, Duebel J, Waters J, Bujard H, Griesbeck O, Tsien RY, Nagai T, Miyawaki A, Denk W. Functional fluorescent Ca^{2+} indicator proteins in transgenic mice under TET control. *PLoS Biol* 2: e163, 2004.

Hendel T, Mank M, Schnell B, Griesbeck O, Borst A, Reiff DF. Fluorescence changes of genetic calcium indicators and OGB-1 correlated with neural activity and calcium in vivo and in vitro. *J Neurosci* 28: 7399–7411, 2008.

Hutzler M, Lambacher A, Eversmann B, Jenkner M, Thewes R, Fromherz P. High-resolution multitransistor array recording of electrical field potentials in cultured brain slices. *J Neurophysiol* 96: 1638–1645, 2006.

Jeon CJ, Strettoi E, Masland RH. The major cell populations of the mouse retina. *J Neurosci* 18: 8936–8946, 1998.

Kettunen P, Demas J, Lohmann C, Kasthuri N, Gong Y, Wong RO, Gan WB. Imaging calcium dynamics in the nervous system by means of ballistic delivery of indicators. *J Neurosci Methods* 119: 37–43, 2002.

Lambacher A, Jenkner M, Merz M, Eversmann B, Kaul RA, Hofmann F, Thewes R, Fromherz P. Electrical imaging of neuronal activity by multi-transistor-array (MTA) recording at 7.8 μm resolution. *Appl Phys A Mater Sci Process* 79: 1607–1611, 2004.

Litke AM, Chichilnisky EJ, Dabrowski W, Grillo AA, Grybos P, Kachiguine S, Rahman M, Taylor G. Large-scale imaging of retinal output activity. *Nucl Instrum Methods Phys Res A* 501: 298–307, 2003.

Meister M, Pine J, Baylor DA. Multi-neuronal signals from the retina: acquisition and analysis. *J Neurosci Methods* 51: 95–106, 1994.

Miyawaki A, Llopis J, Heim R, McCaffery JM, Adams JA, Ikura M, Tsien RY. Fluorescent indicators for Ca^{2+} based on green fluorescent proteins and calmodulin. *Nature* 388: 882–887, 1997.

Morgan JL, Wong RO. Ballistic labeling with fluorescent dyes and indicators. *Curr Protoc Neurosci* Chapter 2: Unit 2.11, 2008.

Nagayama S, Zeng S, Xiong W, Fletcher ML, Masurkar AV, Davis DJ, Pieribone VA, Chen WR. In vivo simultaneous tracing and Ca(2+) imaging of local neuronal circuits. *Neuron* 53: 789–803, 2007.

Oesch N, Euler T, Taylor WR. Direction-selective dendritic action potentials in rabbit retina. *Neuron* 47: 739–750, 2005.

Persechini A, Lynch JA, Romoser VA. Novel fluorescent indicator proteins for monitoring free intracellular Ca^{2+}. *Cell Calcium* 22: 209–216, 1997.

Roe MW, Lemasters JJ, Herman B. Assessment of Fura-2 for measurements of cytosolic free calcium. *Cell Calcium* 11: 63–73, 1990.

Roehlich P, Vanveen T, Szél A. Two different visual pigments in one retinal cone cell. *Neuron* 13: 1159–1166, 1994.

Rols MP, Teissie J. Electropermeabilization of mammalian cells to macromolecules: control by pulse duration. *Biophys J* 75: 1415–1423, 1998.

Schlichtenbrede FC, Mittmann W, Rensch F, Vom Hagen F, Jonas JB, Euler T. Toxicity assessment of intravitreal triamcinolone and bevacizumab in a retinal explant mouse model using two-photon microscopy. *Invest Ophthalmol Vis Sci* 50: 5880–5887, 2009.

Segev R, Goodhouse J, Puchalla J, Berry MJ 2nd. Recording spikes from a large fraction of the ganglion cells in a retinal patch. *Nat Neurosci* 7: 1154–1161, 2004.

Shlens J, Field GD, Gauthier JL, Greschner M, Sher A, Litke AM, Chichilnisky EJ. The structure of large-scale synchronized firing in primate retina. *J Neurosci* 29: 5022–5031, 2009.

Shlens J, Field GD, Gauthier JL, Grivich MI, Petrusca D, Sher A, Litke AM, Chichilnisky EJ. The structure of multi-neuron firing patterns in primate retina. *J Neurosci* 26: 8254–8266, 2006.

Siegert S, Scherf BG, Del Punta K, Didkovsky N, Heintz N, Roska B. Genetic address book for retinal cell types. *Nat Neurosci* 12: 1197–1204, 2009.

Stosiek C, Garaschuk O, Holthoff K, Konnerth A. In vivo two-photon calcium imaging of neuronal networks. *Proc Natl Acad Sci USA* 100: 7319–7324, 2003.

Tsien RY. A non-disruptive technique for loading calcium buffers and indicators into cells. *Nature* 290: 527–528, 1981.

Weng S, Sun W, He S. Identification of ON-OFF direction-selective ganglion cells in the mouse retina. *J Physiol* 562: 915–923, 2005.

Wong RO, Oakley DM. Changing patterns of spontaneous bursting activity of on and off retinal ganglion cells during development. *Neuron* 16: 1087–1095, 1996.

Yaksi E, Friedrich RW. Reconstruction of firing rate changes across neuronal populations by temporally deconvolved Ca^{2+} imaging. *Nat Methods* 3: 377–383, 2006.

Yu J, Daniels BA, Baldridge WH. Slow excitation of cultured rat retinal ganglion cells by activating group I. metabotropic glutamate receptors. *J Neurophysiol* 102: 3728–3739, 2009.

Zhan XJ, Troy JB. An efficient method that reveals both the dendrites and the soma mosaics of retinal ganglion cells. *J Neurosci Methods* 72: 109–116, 1997.